Structure and composition of ε-W_2B_{5-x}

Samaneh S. Setayandeh[1,*], Edward G. Obbard[1], Jennifer H. Stansby[1], Dillon Frost[1], Jack O. Astbury[2], Chris L. Wilson[2] and Patrick A. Burr[1]

[1]School of Mechanical and Manufacturing Engineering, University of New South Wales, Kensington, 2052, NSW, Australia

[2]Tokamak Energy Ltd, 173 Brook Drive, Milton Park, Oxon, OX14 4SD, United Kingdom

There is no consensus in the literature on the structure and composition of the ε phase of the W-B system, variously reported as WB_2 and W_2B_5. We used *ab initio* calculations at two levels of theory to identify the stable crystal structure and stoichiometry of this phase. Among the sixteen structures investigated in the composition range of 67–71.4 at. % B (WB_2–W_2B_5), nine exhibited unfeasibly high formation energies; the remaining seven were dynamically stable (did not exhibit any soft phonon modes), and satisfied mechanical stability criteria. When including the thermal vibrational contribution to the free energy, all structures with the W_2B_5 composition lied above the convex hull, suggesting that this composition is metastable, while those with WB_2 composition lied on the convex hull or within DFT accuracy of the convex hull. We found that four of the candidate structures exhibit negative vacancy formation energy, suggesting that the structures are unstable, or that they are naturally hypo-stoichiometric. Combining these results with a comparison of simulated and experimental x-ray and neutron diffraction patterns, we concluded that the ε phase is most likely a hypo-stochiometric W_2B_{5-x} compound with space group $P6_3/mmc$.

Keywords: tungsten boride**,** *ab initio* calculations, neutron diffraction, X-ray diffraction

* Corresponding author. School of Mechanical and Manufacturing Engineering, University of New South Wales, Kensington, 2052, NSW, Australia. E-mail address: s.setayandeh@unsw.edu.au

1. Introduction

Tungsten borides are a class of ultra-hard high temperature ceramics (Vickers hardness ≈ 42 GPa for tungsten tetraboride[1]), with outstanding physical and chemical properties, including chemical inertness, thermal shock and high-temperature electrical resistance [2-4] that compete with those of traditional hard materials [5-12]. The rich array of physical behaviours of tungsten borides has made them strong candidates for refractory and high temperature applications [13-18]; and recently they have been highlighted as promising candidate materials for radiation shielding of nuclear fusion applications [19, 20]. In particular, the spherical tokamak reactor design [21] has limited space between the high energy fusion plasma and the cryogenically-cooled superconducting magnets, and therefore require materials with exceptional shielding performance, offered by tungsten borides [22].

The first complete report of phase diagram of the tungsten-boron system can be traced back to 1963 by Kieffer *et al* [23]. Since then, five phases have been identified for the W-B system: W_2B (γ phase) [24, 25], WB, (variously reported as α or β phase) [24, 26], WB_2 ($A1B_2$-type structure) [27], W_2B_5 (ε phase) [24, 28] and WB_4 [29]. Determination of crystal structures of these compounds, especially boron-rich compounds (B > 50 %), has been challenging and in some cases it remains unclear [30]. This is partly because atomic scattering factor of x-rays scales with Z^2, so structure factors are dominated by W (Z=74), with low sensitivity to occupancy or position of B (Z=5). Neutron scattering, on the other hand, is challenging due to the high cross-section for neutron absorption of B-10.

For the ε phase in particular, not only is the structure uncertain [8], but the composition has also been reported across a range spanning 65–71.4 at. % B, such as W_2B_5 [24], WB_2 (W_2B_4) [8, 31], $WB_{2.27}$ [32],W_2B_{5-x} [26] and W_2B_{4-x} [33]. The first report of the ε phase was by Kiessling in 1947 [24], who reported a composition of W_2B_5 (71.4 at. % B) and a hexagonal crystal structure with space group $P6_3/mmc$, obtained from single crystal X-ray diffraction. The proposed structure comprises two types of boron layers: a graphite-like planar layer and a six-membered zig-zag layer with one boron atom located in the centre (see Figure 1a). Later work by Frotscher *et al.* in 2007 [8] indicated that the ε phase is better described by a W_2B_4 composition (66.7 at. % B), in which the boron atom site in the center of the six-membered zig-zag layer is removed (Figure 1b). However, the experimental results from neutron diffraction remained inconclusive [8]. Kayhan *et al.* in 2013 [33], proposed a new composition, W_2B_{4-x}, with space group $P6_3/mcm$ based on the neutron diffraction, in which a further boron atom was partially removed (occupancy of 0.166) in the graphite-like layers. However, this proposed composition (62 at. % B) deviates significantly from the density measurements reported by Kiessling (71.4 at. % B). The proposed structure was largely based on relative intensity of the neutron diffraction peaks [33], and therefore would be strongly sensitive to sample texture, perhaps explaining part of the disagreement.

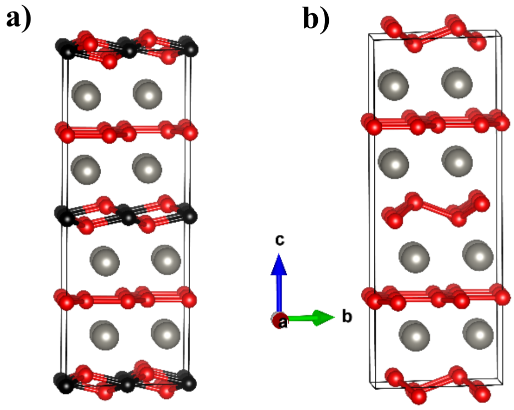

Figure 1. Unit cells of a) W_2B_5 structure suggested by Kiessling [24], and b) W_2B_4 reported by Frotscher et al. [8], both with space group P6$_3$/mmc. Large grey atoms are W and small red atoms are B. Small black atoms in panel **a** are B atoms located in the centre of the six-membered zig-zag layers.

Overall, the exact composition and atomic coordinates of the ε phase remain unclear. Due to the technological importance of boron-rich tungsten borides, and specifically for neutron shielding applications where the performance is strongly sensitive to the boron atomic density, it is a pressing task to resolve this question unambiguously. Here we use ab-initio calculations to identify the crystal structure and stoichiometry in the W-B system. We assess phase stability based on thermodynamics, lattice dynamic, mechanics and point defect chemistry, in the temperature range 0-2500 K. For the most promising candidates, we report the calculated x-ray and neutron diffraction patterns and elastic constants to aid further experimental studies.

2. Methodology

All DFT simulations were carried out using the Vienna Ab-Initio Simulation Package (VASP) [34-36], using two exchange correlation functionals: the local density approximation (LDA) [37] and the Perdew, Burke, and Ernzerhof (PBE) formulation of the generalised gradient approximation [38]. Where only one set of results is reported, it is for the PBE functional unless stated otherwise. Atoms were described with PAW pseudo-potentials [39, 40] from the VASP 5.3 repository with three and six valence electrons for B and W respectively and a consistent plane-wave cut-off of 400 eV. The Monkhorst-Pack method [41] was applied to sample the electronic wave functions in Brillouin zone on a k point grid with a density of 31.4 Å in all directions, which produced results converged to $\pm 10^{-2}$ eV compared to a highly dense grid (47

Å). Partial occupancies were treated with a first-order Methfessel-Paxton smearing function of width 0.1 eV [42]. All structures were optimised by relaxing their lattice parameters and internal atomic coordinates. The formation enthalpy per atom, E_f, was calculated as:

$$\Delta E_f = \frac{\mu(\mathrm{W}_x\mathrm{B}_y) - x\mu(\mathrm{W}) - y\mu(\mathrm{B})}{x+y} \quad (1)$$

where μ is the chemical potentials of the compound and reference phases. In the first instance this is taken to be the DFT total energy of a unit cell containing x W and y B atoms for the boride, and half the DFT energy of a tungsten bcc unit cell and one thirty-sixth of the DFT energy of an α-B unit cell for $\mu(\mathrm{W})$ and $\mu(\mathrm{B})$, respectively. For a more complete description of the formation energy, we also consider the vibrational energy and vibrational entropy contributions ($\Delta F^{vib} = \Delta E^{vib} + T\Delta S^{vib}$) to the stability of the boride. Thus, the formation free energy per atom, F_f, was similarly calculated as:

$$\Delta F_f = \Delta E_f + \Delta F^{vib} \quad (2)$$

where F^{vib} is calculated from the phonon frequencies (ω_i) at temperature T within the harmonic approximation, via a supercell approach, as [43]:

$$F^{vib} = \frac{1}{2}\sum_i^{3N} \hbar\omega_i + k_B T \sum_i^{3N} \ln\left(1 - e^{\frac{-\hbar\omega_i}{k_B T}}\right) \quad (3)$$

where k_B and N stand for the Boltzmann constant and number of atoms, respectively. The dynamical matrices for the phonon calculations [44] were computed using the Phonopy package [45].

Elastic constants were obtained by applying displacements of ± 0.01Å and ± 0.02Å in each symmetrically independent direction of the crystal. The elastic constants were fitted to the response of energy and atomic forces to the applied displacements, following the algorithm built into VASP [34-36]. The effect of ionic relaxation on elastic constants was also taken into account, although it was never greater than 4.7 % of the primary stiffness constants. Bulk and Shear moduli were obtained assuming a polycrystalline aggregate, as described in the Hill method [46] of averaging Voight [47] and Reuss [48] bounding cases.

Formation enthalpy of dilute point defect was calculated as:

$$E_{Defect} = E_{tot}(\mathrm{Defect}) - E_{tot}(\mathrm{Perfect}) - \sum n_i \mu_i \quad (4)$$

where $E_{tot}(\mathrm{Defect})$ and $E_{tot}(\mathrm{Perfect})$ are the total energy of the supercell with one defect and its equivalent perfect supercell, respectively. n_i and μ_i denote the number of atoms i removed from ($-n_i$) or added to ($+n_i$) the supercell to form the defect, and their corresponding chemical potential, respectively. The XRD and neutron data simulations were carried out by application of GSAS-II software [49].

3. Results and Discussion

3.1. Thermodynamic stability

Twenty-three reported polymorphs of tungsten boride (W_xB_y), in the composition range of 50–80 at. % B, were investigated. The stability of all structures was quantified via calculation of formation enthalpy per atom (eqn. 1) at ground state, with the PBE exchange-correlation functional. These are presented in figure 2 in the form of a convex hull. In principle, any compound whose formation enthalpy lies on the convex hull is thermodynamically stable and any that does not is deemed metastable [50, 51]. Among the sixteen structures investigated in the composition range of 67–71.4 at. % B (WB_2–W_2B_5), seven lower energy compounds were selected for further investigation, and their formation enthalpy was calculated also using the LDA exchange-correlation functional (Figure 2b). These selected compounds are depicted in figure 3 and their crystal structures are described in Table 1. The results from the two levels of theory are in remarkable agreement, with only small changes that are within the expected level of accuracy of DFT, suggesting that the results are insensitive to the choice of exchange correlation function. Among these seven compounds, the compounds of WB_2 composition are closer to the convex hull than the compounds of W_2B_5 composition. None of the compounds of W_2B_5 composition (W_2B_5 (P6₃/mmc) and W_2B_5 (R3m) lies on the calculated convex hull, suggesting that this composition is metastable.

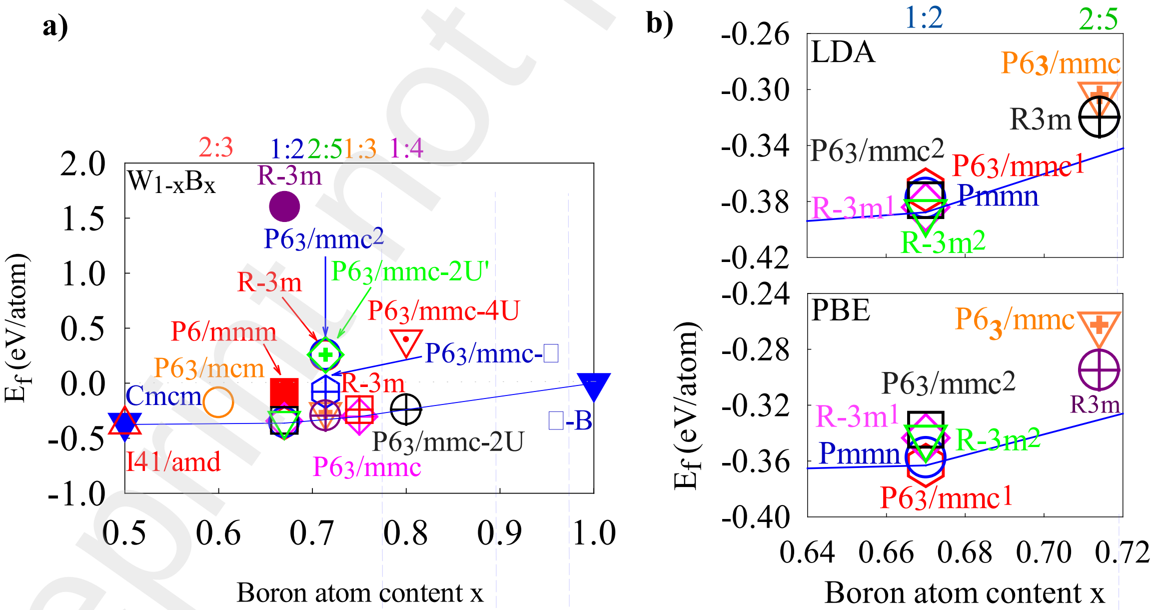

Figure 2. a) Convex hull diagram for the B-rich side of the W-B system, obtained with the PBE exchange correlation functionals. Panel b) illustrates the region around the ε phase obtained with the PBE and LDA.

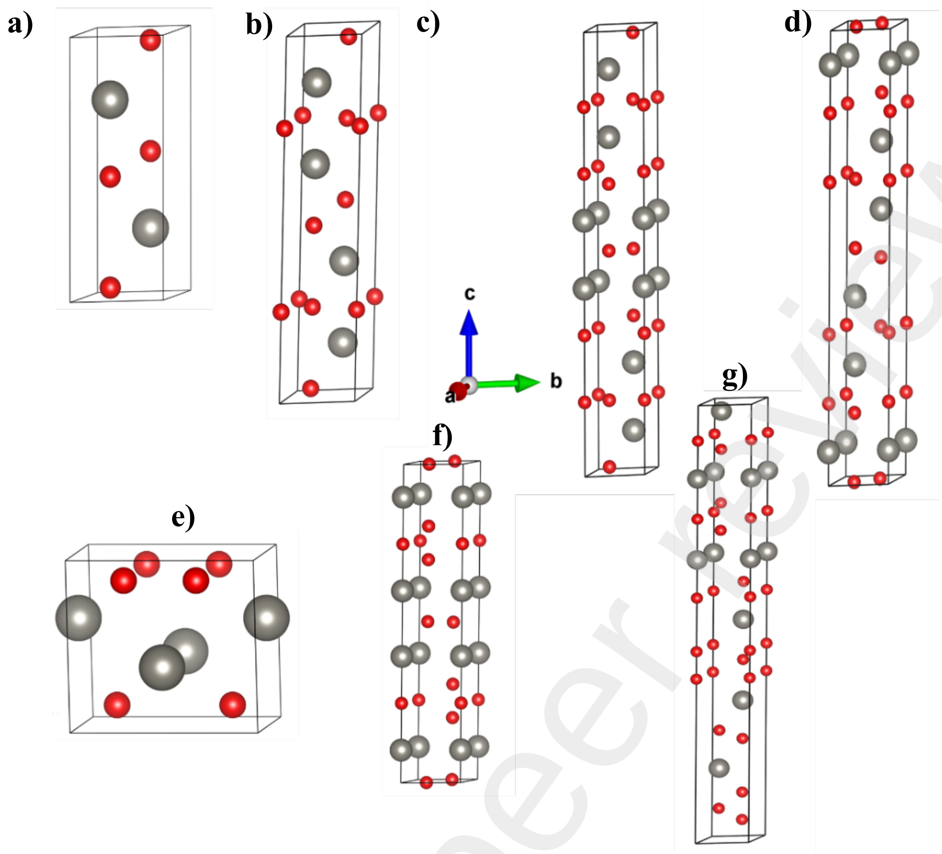

Figure 3. Unit cell representations of the lowest-energy candidate structure of the ε phase: (a) WB_2 ($P6_3/mmc^1$) [30], (b) WB_2 ($P6_3/mmc^2$)[8], (c) WB_2 ($R\text{-}3m^1$)[30], (d) WB_2 ($R\text{-}3m^2$)[8], e) WB_2 (Pmmn)[30], f) W_2B_5 ($P6_3/mmc$)[30] and g) W_2B_5 (R3m)[52]. Grey/large atoms are W and red/small atoms are B. A superscript ^{1} or ^{2} indicate variations of the crystal with the same space group but different motif.

Table 1. Crystal structure definition and formation enthalpies (per atom) of lowest-energy candidate structure of the ε phase. E_f reported from PBE calculations and, in square brackets, from LDA calculations.

Comp.	Space group	E_f (eV/atom)	Lattice Parameter (Å)	Wyckoff positions				Ref.
				Atom	x	y	z	
WB_2	$P6_3/mmc$[1] (Hexagonal)	-0.3632 [-0.3718]	a= 2.9269 c= 7.7507	W (2c)	0.333333	0.666667	0.250000	[30]
				B (4f)	0.333333	0.666667	0.540730	
	$P6_3/mmc$[2] (Hexagonal)	-0.3376 [-0.3790]	a=2.9840 c=13.8700	W1(4f)	0.333333	0.666667	0.139000	[8]
				B1 (4f)	0.333333	0.666667	-0.028000	
				B2(2d)	0.333333	0.666667	0.750000	
				B3(2b)	0.000000	0.000000	0.250000	
	R-3m[1] (Rhombohedral (I))	-0.3435 [-0.3841]	a=3.0135 c=21.0948	W (6c)	0.000000	0.000000	0.576430	[30]
				B1(6c)	0.000000	0.000000	0.681720	
				B2 6c)	0.000000	0.000000	0.168050	
	R-3m[2] (Rhombohedral (I))	-0.3434 [-0.3878]	a=3.0138 c=20.9541	W (6c)	0.000000	0.000000	0.075100	[8]
				B1(6c)	0.000000	0.000000	0.332900	
				B2(6c)	0.000000	0.000000	0.181000	
	Pmmn (Orthorhombic)	-0.3575 [-0.3776]	a= 2.9187 b=4.6563 c= 4.2308	W1(2b)	0.000000	0.500000	0.379780	[30]
				B1(4e)	0.000000	0.692610	0.884460	
W_2B_5	$P6_3/mmc$ (Hexagonal)	-0.2624 [-0.3038]	a= 3.0171 c=15.7082	W1(4e)	0.000000	0.000000	0.397090	[30]
				B1(2b)	0.000000	0.000000	0.250000	
				B2(4f)	0.333333	0.666667	0.302580	
				B3 (4f)	0.333333	0.666667	0.497260	
	R3m (Trigonal)	-0.2949 [-0.3197]	a= 2.9225 c= 5.9018	W1(3a)	0.666667	0.333333	0.981200	[52]
				W2(3a)	0.666667	0.333333	0.165900	
				B1 (3a)	0.666667	0.333333	0.074200	
				B2 (3a)	0.666667	0.333333	0.252500	
				B3 (3a)	0.333333	0.666667	0.042200	
				B4 (3a)	0.333333	0.666667	0.104900	
				B5(3a)	0.333333	0.666667	0.227300	

The ground-state calculations presented above were extended to include thermal effects by performing phonon simulations for the seven most promising structures and calculating the vibrational free energy within the harmonic approximation (eqn. 3). Figure 4 shows the formation free energy of these structures at 300 K and 2500 K, obtained with the PBE and LDA exchange correlation functionals (via eqn. 2). A comparison between the formation enthalpy of these compounds at their ground state (Figure 2) and higher temperatures indicates that inclusion of vibrational energy does not change the higher stability of WB_2 compounds compared to the W_2B_5 compounds. However, the order of stability of compounds within the WB_2 composition is somewhat affected by vibrational energy: at room temperature both WB_2 ($P6_3/mmc^1$) and WB_2 ($R\text{-}3m^2$) structures remain within DFT accuracy of the convex hull (as per the ground state), while at high temperature (2500 K), WB_2 ($R\text{-}3m^2$) appears to be metastable.

Figure 4 shows temperature dependences of the formation free energy of different compounds of WB_2 and W_2B_5 compositions, obtained with the LDA and PBE functionals. The cross-over in stability occurs around 1300 K, however, for four compounds (W_2B_5 ($P6_3/mmc$), W_2B_5 (R3m), WB_2 ($P6_3/mmc^1$) and WB (Pmmn)) the range of formation energies remains within the bounds of uncertainty of DFT calculations. Note also that the harmonic approximation used here does not include the effect of thermal expansion, the presence of defects, and anharmonic effects, none of which are expected to play a significant role until elevated temperature, and unlikely to be significant at 300 K. Overall, no significant changes are observed in the metastability of the compounds of W_2B_5 composition, as they lie above the convex hull at all temperatures.

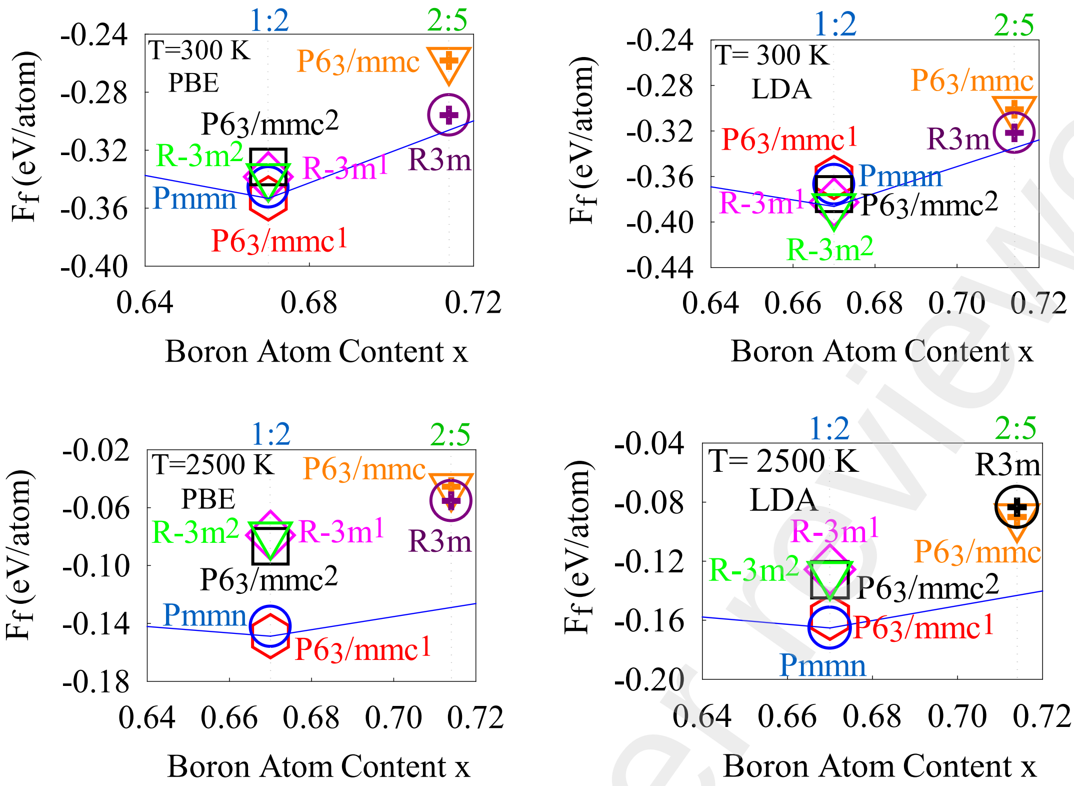

Figure 5. Formation free energy of different compounds of WB_2 and W_2B_5 compositions, obtained with the PBE and the LDA exchange correlation functionals at different temperatures.

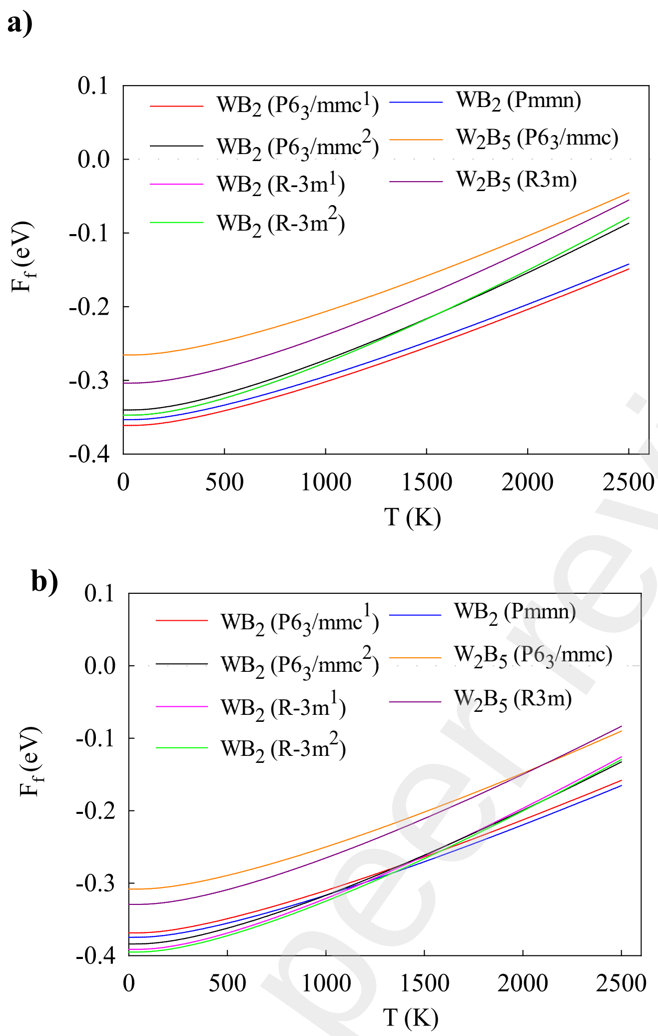

Figure 6. Temperature dependences of the formation free energy of different compounds of WB_2 and W_2B_5 compositions, obtained with the a) PBE and b) LDA exchange correlation functionals.

3.2. Dynamical and Mechanical Stability

To investigate dynamic stabilities of structures considered, phonon calculations were carried out. It is well established that the PBE (LDA) exchange correlation functional produces higher (lower) values of lattice parameters than experimental values, and for some materials with significant mass difference in the constituent elements (e.g. PdH) [53] this can affect the phonon results drastically. For this reason, we repeat the calculations at both levels of theory. Figure 6 shows the results of the phonon calculations with both PBE (solid blue) and LDA (dashed black) functionals. Both approximations lead to essentially identical results, except for a small shift to higher frequencies of LDA, as expected from the slightly reduced lattice parameters. Importantly, no soft modes are present in the phonon dispersion curves of all structures of interest, with both levels of theory, which is a strong sign of dynamic stability.

The elastic constants (c_{ij}) of the candidate structures are reported in Table 2. All structures satisfied the Born-Huang mechanical stability criteria [54-57]. All candidate structures exhibit stiff constants, in excess of 500 GPa for c_{11}, c_{22} and c_{33}. Notably, the WB_2 ($P6_3/mmc^1$) structure possesses a remarkably high value of c_{33} (≈ 950 GPa), indicating a stiffness along the *c* axis akin to diamond ($c_{ij}^{diamond} \approx 1000$ GPa) [58, 59]. For all structures, c_{11} and c_{44} are not equal to c_{33} and c_{66}, respectively, indicating elastic anisotropy [60].

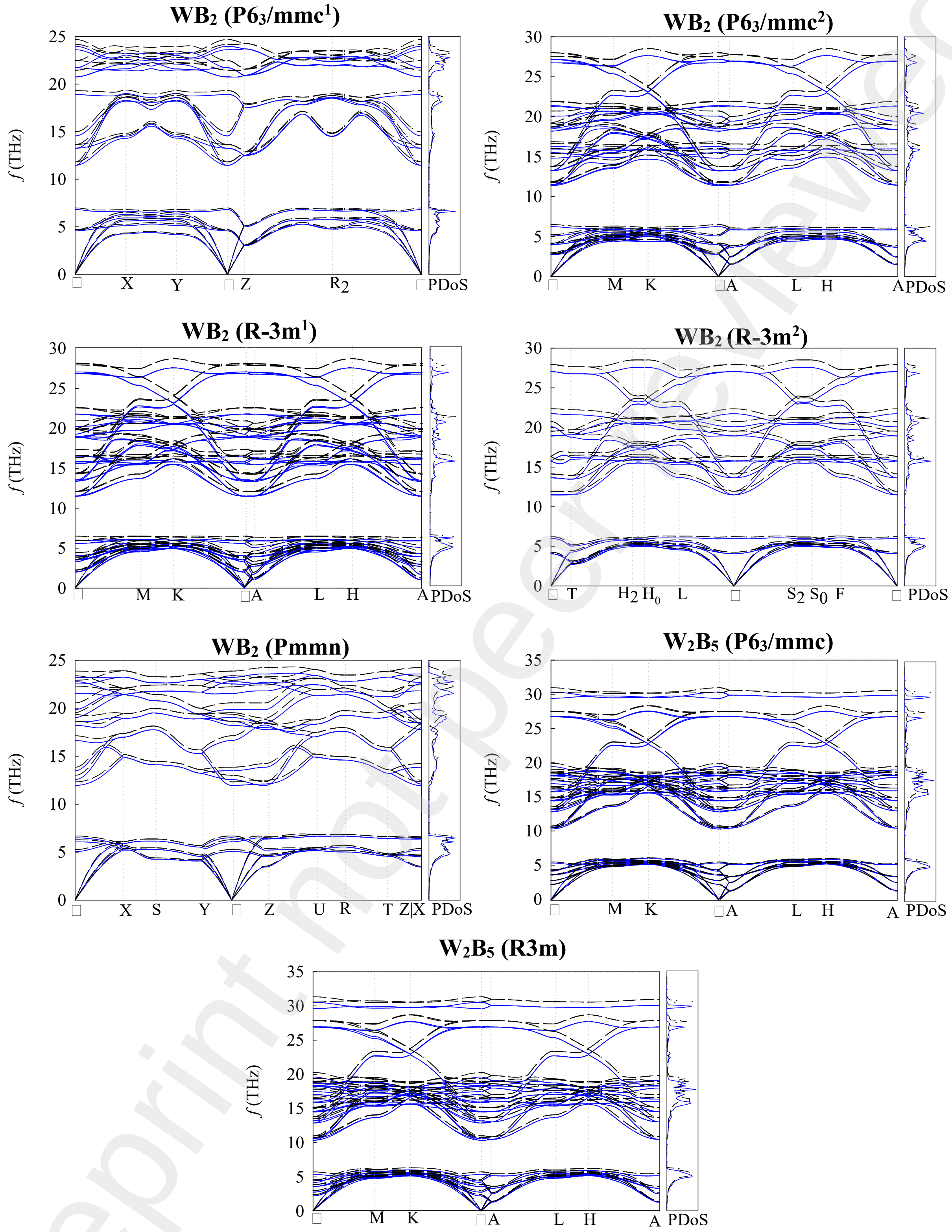

Figure 7 Phonon band structure and density of state of candidate structures of the ε phase, obtained with the PBE (blue/solid lines) and LDA (black/dashed lines) exchange-correlation functionals.

Table 2 Calculated elastic constants c_{ij} (in GPa) for the seven leading candidate structures of the ε phase.

Structure	c_{11}	c_{22}	c_{33}	c_{12}	c_{13}	c_{23}	c_{44}	c_{55}	c_{66}
WB_2 ($P6_3/mmc^1$)	591.3	591.8	953.4	174.6	106.4	106.2	283.9	283.8	208.2
WB_2 ($P6_3/mmc^2$)	612.8	612.8	726.3	149.9	26.44	186.2	230.6	230.6	231.4
WB_2 (R-3m[1])	596.1	596.1	701.2	146.4	202.3	202.3	237.6	237.6	224.9
WB_2 (R-3m[2])	596.5	596.5	702.2	146.5	202.1	202.1	237.8	237.8	225.0
WB_2 (Pmmn)	570.0	514.6	875.6	217.3	72.75	171.5	196.9	313.7	242.0
W_2B_5 ($P6_3/mmc$)	559.2	559.2	698.2	159.2	200.1	200.1	212.6	212.6	200.0
W_2B_5 (R3m)	556.6	556.6	838.9	147.0	152.4	152.4	277.6	277.6	204.8

The bulk modulus (B), shear modulus (G), Poisson's ratio (υ) [61], Pugh's modulus ratio (G_H/B_H) [62] and Cauchy pressure ($c_{12} - c_{44}$) [63, 64] of polycrystalline aggregates here were calculated from the elastic constants, and are reported in Table 3. WB_2 ($P6_3/mmc^2$) possesses the most incompressibility (B ~ 350 GPa) and accordingly the strongest W-d and B-p orbital hybridization among all other candidates [65]. Conversely, WB_2 ($P6_3/mmc^1$) has the highest shear resistance, of about 275.2 GPa. For all candidates except WB_2 (Pmmn), the values of υ and Cauchy pressure are less than 0.26 and 0, respectively, which together with the positive value of G_H/B_H, indicate brittleness of these structures. Figure 7 shows calculated bulk modulus (B), shear modulus (G) and Poisson's ratio (υ) of these candidates, graphically.

Cheng *et al*. [59] found a strong correlation between mechanical properties and thermodynamic stability of the W-B system, claiming the compound with the lowest formation energy for a given composition possesses the smallest Poisson's ratio and the largest shear modulus. Such strong correlations were also observed in our calculations.

In the next section we explore the ability of the proposed structures to accommodate deviations of stoichiometry through point defects.

Table 3 Bulk modulus from Hill average (B_H) of Voigt (B_V) and Reuss (B_R) moduli, and same for Shear modulus, G, Poisson's ratio (υ), Pugh's modulus ratio (G_H/B_H), and Cauchy pressure $c_{12} - c_{44}$ of the leading candidate structures of the ε phase.

Structure	Bulk modus (GPa)			Shear modulus (GPa)			υ	G_H/B_H	$c_{12} - c_{44}$
	B_H	B_V	B_R	G_H	G_V	G_R			
WB_2 ($P6_3/mmc^1$)	316.3	320.2	312.5	275.2	285.4	265.0	0.1628	0.8700	-109.3
WB_2 ($P6_3/mmc^2$)	350.0	329.6	370.4	242.4	245.5	239.2	0.2187	0.6925	-80.7
WB_2 ($R\text{-}3m^1$)	321.0	329.5	312.5	237.0	241.0	232.9	0.2038	0.7382	-91.2
WB_2 ($R\text{-}3m^2$)	331.5	329.6	333.3	236.4	241.2	231.5	0.2120	0.7130	-91.3
WB_2 (Pmmn)	314.9	317.2	312.7	249.0	263.0	235.1	0.1871	0.7907	20.4
W_2B_5 ($P6_3/mmc$)	313.0	322.9	303.0	218.0	224.2	211.9	0.2173	0.6966	-53.3
W_2B_5 (R3m)	295.9	314.1	277.8	256.7	264.6	248.8	0.1636	0.8674	-130.6

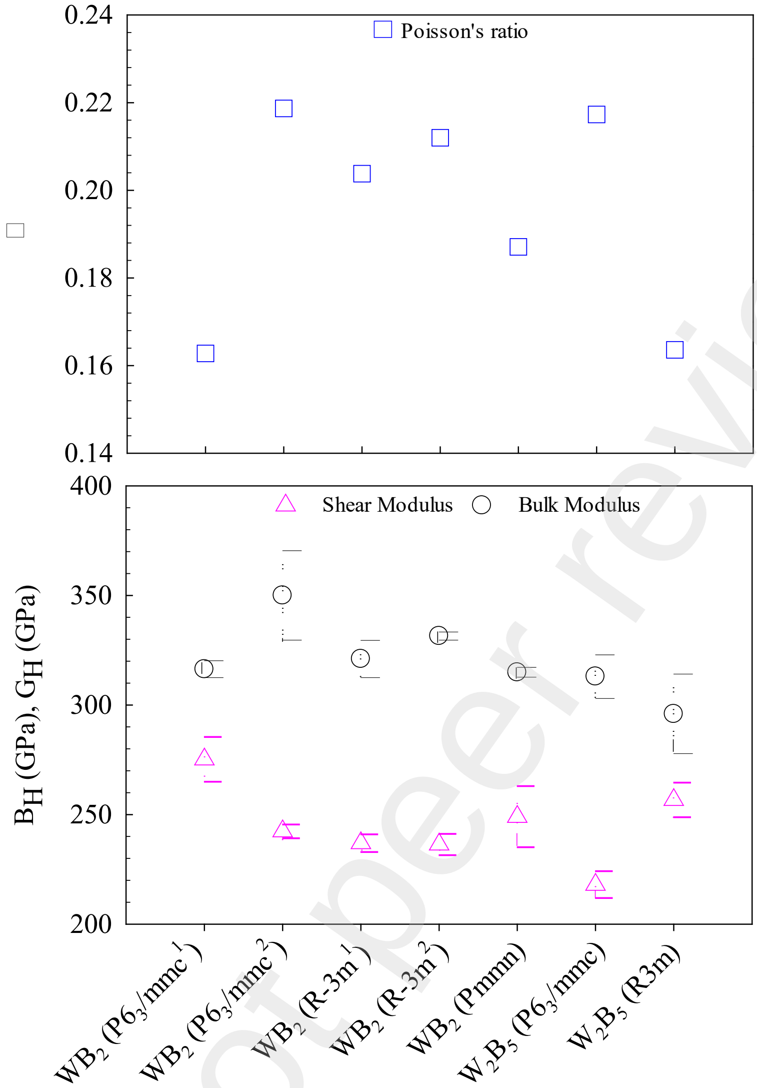

Figure 8 Poisson's ratio (top panel), bulk and shear moduli (bottom panel) of the leading candidate structures of the ε phase. The error bars represent the range between Reuss and Voight values and the symbols indicate the average (Hill value).

3.4 Dilute point defect

Deviation of stoichiometry may be accommodated by interstitials, vacancies, and anti-site defects. Specifically, the presence of W vacancies and B interstitials leads to hyper-stoichiometry (boron-rich compositions) while B vacancies lead to hypo-stoichiometry (boron-poor compositions). W interstitial would also lead to hypo-stoichiometry, however these are very large defects that are likely to have large associated energy (as observed for in WC [66] and for uranium interstitials in the related compound UB_2 [67]). Similarly, anti-site defects (W on B site and vice-versa) are unlikely to be easily accommodated in tungsten borides. Figure 8 shows the formation enthalpy of tungsten and boron interstitials, and tungsten vacancies for the structures considered in this study.

Negative vacancy formation energies are observed for four structures: WB_2 ($P6_3/mmc^2$), WB_2 ($R\text{-}3m^1$), WB_2 ($R\text{-}3m^2$) and W_2B_5 ($P6_3/mmc$). This implies that the defects would form spontaneously, and is clear sign of structural instability of the stoichiometric compound. The ability to accommodate large deviations of stoichiometry is usually manifest in a small but positive formation energy of the defect through which the deviation is accommodated. However, a negative defect formation could also indicate a strong drive toward non-stoichiometry, provided that the addition of further defects leads, eventually, to an increase in the defect formation energy above zero. The negative formation energy of defects for the WB_2 ($P6_3/mmc^2$) and WB_2 ($R\text{-}3m^1$) structures is in good accordance with their formation enthalpies, which lie well above the free energy convex hulls (Figure 2a), indicating their metastability. On the other hand, WB_2 ($R\text{-}3m^2$) structure is found to be within DFT accuracy of the convex hull, and combining this with the negative formation of B2 vacancies, it would suggest that if the compound were stable it would have to have a significantly reduced stoichiometry from that reported experimentally. Finally, for W_2B_5 ($P6_3/mmc$), while it has a free energy of formation significantly above the convex hull, this reduces significantly when a concentration of B vacancies is added to the structure, each with an associated formation energy of –0.578eV, and concurrently reducing the stoichiometry closer to the more commonly reported values. Whether the reduction in energy through the introduction of vacancies is sufficient to stabilise the structure cannot be said without a further dedicated study.

For five structures there are multiple distinct boron sites (denoted by a number in Figure 8), each with a different vacancy formation energy. In the case of WB_2 ($P6_3/mmc^2$), WB_2 ($R\text{-}3m^1$), WB_2 ($R\text{-}3m^2$) and W_2B_5 ($P6_3/mmc$), one of these displays negative formation energy, while the others exhibit positive formation energy. For the W_2B_5 ($R3m$) structure, five symmetrically distinct sites exhibit, however their formation energies fall on of two energy levels, due to similar local environments: vacancies on site 3 and 4 have $E_{Defect} = 2.2$ eV and those on site 1, 2 and 5 have $E_{Defect} =$ 3.5 eV.

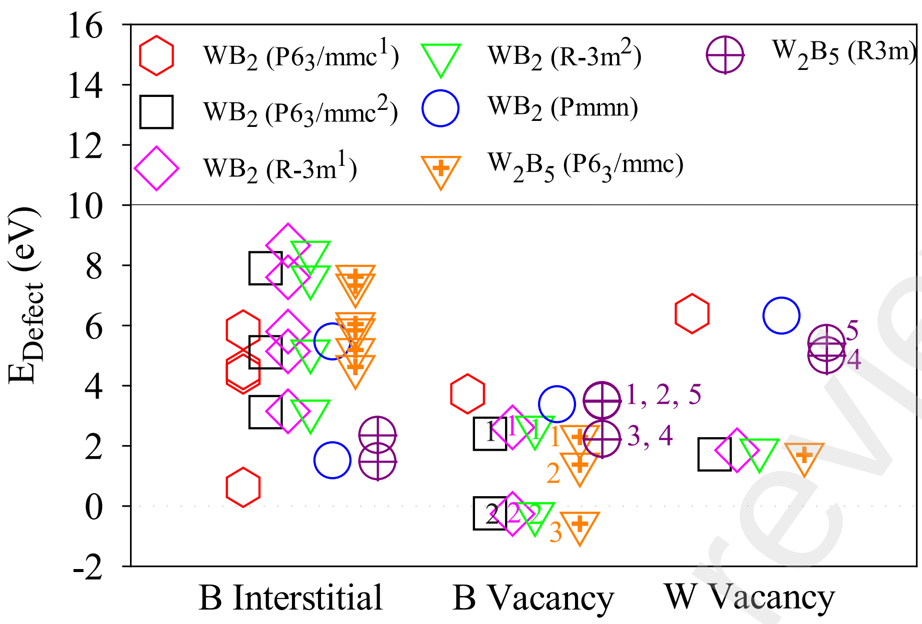

Figure 9 Formation energies of point defects the leading candidate structure of the ε phase. Where multiple non-equivalent sites exist for vacancies, these are denoted by numbers (e.g. B1 of Table 1 denoted as 1).

3.5 XRD and Neutron Diffraction Simulations

Figures 9 and 10 illustrate simulate x-ray (λ=1.5418 Å) and neutron (λ=1.54816 Å) diffraction patterns for the structures of interest, respectively, compared to available experimental data for the ε phase [28, 33]. The experimental XRD and neutron patterns of the ε phase are best fit by WB_2 ($P6_3/mmc^2$). However, this structure lies well above the convex hull, possesses negative formation enthalpy of point defects together with anomalous elastic properties. This indicates that the true structure may perhaps be a variation of WB_2 $P6_3/mmc^2$, with a similar long-range order but different local environment, perhaps akin to that of other candidate structure that lie on the convex hull. It must be stressed that one expects some degree of disagreement between DFT lattice parameter and experiment, typically within 5%, which would move all reflection by varying degree. Even so, it can be stated with confidence that the reflections of the Pmmn space group are incompatible with the experimental ones, while the space groups R-3m and $P6_3/mmc$ both provide reasonable starting point for further refinement.

Neither of the metastable compounds of W_2B_5 ($P6_3/mmc$ and R3m) exhibit convincing diffraction patterns, in agreement with the DFT observation that this composition is metastable. However, since the free energy of W_2B_5 ($P6_3/mmc$) reduces significantly when a concentration of B vacancies is added to this structure, simultaneously reducing its stoichiometry, the true experimental structure might be a variation of this structure with a similar space group where either the boron sites occupancy or the stacking of layers is slightly different. To further advance our understanding of this structure, a new set of accurate neutron diffraction measurements of the ε phase, with B-11 enrichment, high chemical purity and high resolution, is required to confirm and refine the position and occupancy of the boron atoms for this structure.

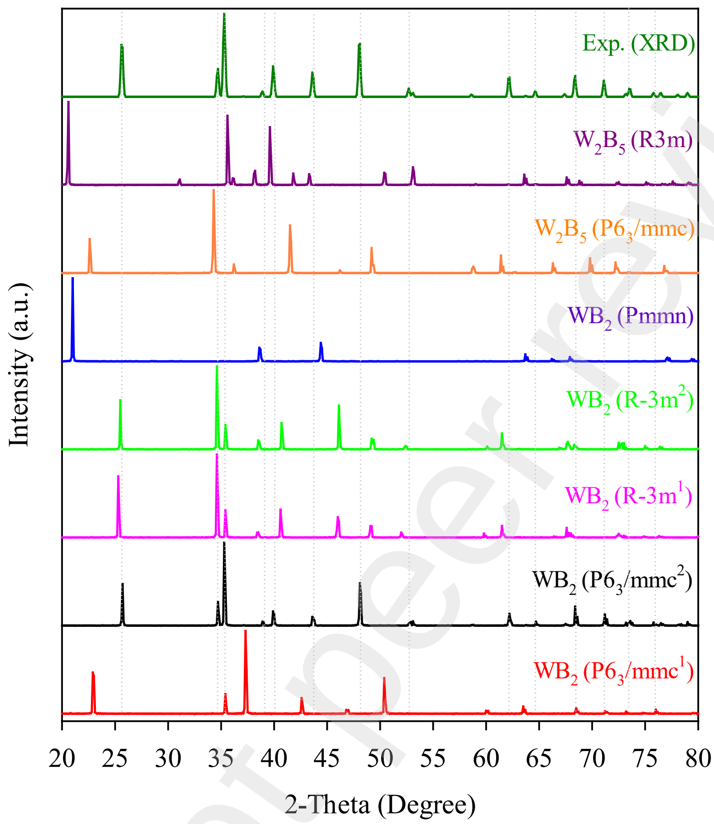

Figure 10 Simulated XRD patterns of the leading candidate structure of the ε phase, including the experimental data of Kayhan et al. [28, 33].

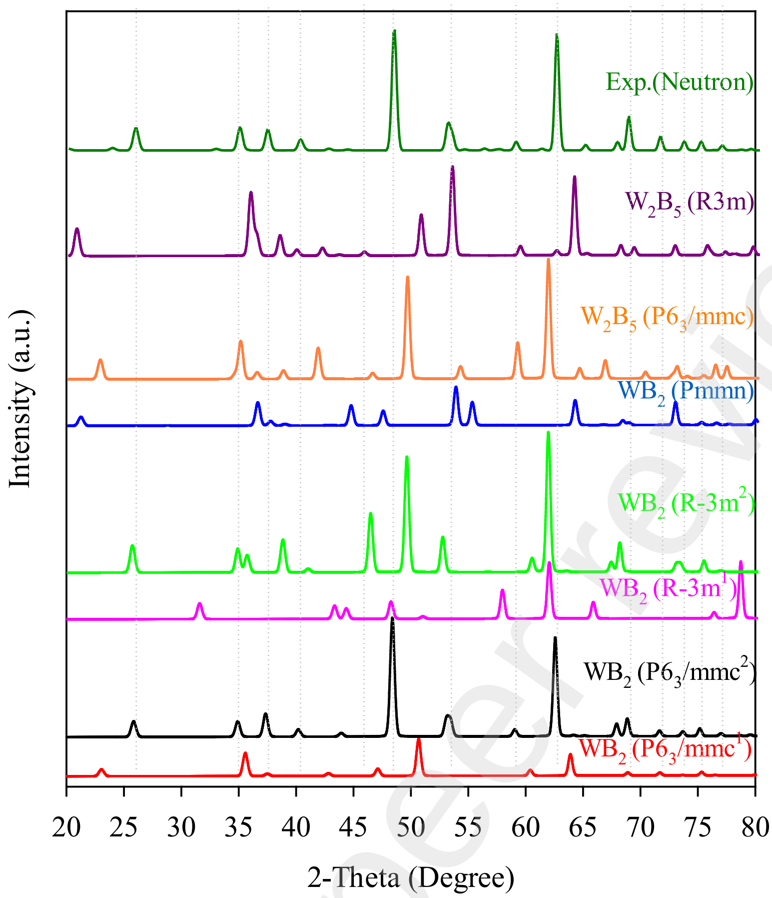

Figure 11 Simulated neutron patterns of the leading candidate structures of the ε phase, including the experimental data of Kayhan et al. [28, 33].

4. Conclusions

DFT calculation were undertaken to identify the structure and composition of the ε phase of tungsten boride. From a starting pool of 16 potential structures in the composition range of 67–71.4 at. % B (WB_2–W_2B_5), seven were found to be promising candidates for this phase on the basis of a convex hull analysis of the free energy of formation, including vibrational thermal contributions. The seven candidates are: WB_2 ($P6_3/mmc^1$), WB_2 ($P6_3/mmc^2$), WB_2 ($R\text{-}3m^1$), WB_2 ($R\text{-}3m^2$), WB_2 (Pmmn), W_2B_5 ($P6_3/mmc$) and W_2B_5 (R3m).

All seven structures were found to be dynamically stable (no soft phonon modes) and mechanically stable (satisfied Born-Huang criteria). All candidates, are predicted to be stiff (bulk moduli 300-350 GPa), brittle and display significant elastic anisotropy.

We considered the possibility that the ε phase may in fact be non-stoichiometric by calculating the point defect formation energy for all candidate structures. Four structures exhibited negative vacancy formation energy: WB_2 ($P6_3/mmc^2$), WB_2 ($R\text{-}3m^1$), WB_2 ($R\text{-}3m^2$) and W_2B_5 ($P6_3/mmc$), suggesting that these structures are either unstable, or the true nature of these compounds is hypo-stoichiometric (boron-deficient). However, in the case of WB_2 compounds, this would take the overall composition far from experimental observation, while in the case of W_2B_5 ($P6_3/mmc$) it would bring it in closer agreement. Comparing simulated diffraction patterns of the candidate structures with experimental x-ray and neutron diffraction measurements, it is evident that the Pmmn space group is incompatible with experimental diffraction patterns, while $P6_3/mmc$, R-3m and R3m are plausible.

We propose that the true experimental structure of the ε phase might be a non-stoichiometric W_2B_{5-x} composition with space group $P6_3/mmc$, which would provide good agreement with available XRD and neutron diffraction measurement, as well as the DFT results of this study.

Acknowledgements

SSS, PAB and EO would like to thank Tokamak Energy (UK) for providing financial support. This research was supported by an Australian Government Research Training Program (RTP) Scholarships. This work was undertaken with the assistance of resources and services from the National Computational Infrastructure (NCI), which is supported by the Australian Government; the Multi-modal Australian Science Imaging and Visualisation Environment (MASSIVE); the Pawsey Supercomputing Centre, which is supported by the Australian Government and the Government of Western Australia; and was enabled by Intersect Australia Limited. Learn more at www.intersect.org.au.

References

1. Gonzalez Szwacki, N., *The structure and hardness of the highest boride of tungsten, a borophene-based compound.* Scientific Reports, 2017. **7**(1): p. 4082.
2. Yazici, S. and B. Derin, *Double SHS of W2B5 Powder from CaWO4 and B2O3.* Advances in Science and Technology, 2010.
3. Funke, V.F., S.l. Yudovskii, and G.V. Samsonov, *Hard Alloys.* Metallurgizdat, 1962. **92**(4).
4. Matkovich, V.I., *Boron and Refractory Borides*. 1977, New York: Springer-Verlag.
5. Zhao, E., et al., *Phase stability and mechanical properties of tungsten borides from first principles calculations.* Physical Chemistry Chemical Physics, 2010. **12**(40): p. 13158-13165.
6. Zhang, R.F., et al., *Stability and Strength of Transition-Metal Tetraborides and Triborides.* Physical Review Letters, 2012. **108**(25): p. 255502.
7. Gou, H., et al., *Peculiar structure and tensile strength of WB4: nonstoichiometric origin.* 2012. **2**(1): p. 012171.
8. Frotscher, M., et al., *M2B5 or M2B4? A Reinvestigation of the Mo/B and W/B System.* 2007. **633**(15): p. 2626-2630.
9. Liang, Y., X. Yuan, and W. Zhang, *Thermodynamic identification of tungsten borides.* Physical Review B, 2011. **83**(22): p. 220102.
10. Chen, X.-Q., et al., *Electronic and Structural Origin of Ultraincompressibility of 5d Transition-Metal Diborides MB_2 (M=W, Re, Os).* Physical Review Letters, 2008. **100**(19): p. 196403.
11. Gromilov, S.A., et al., *Investigation of W2B and β-WB high-temperature phases in coatings produced by a shaped charge explosion.* Journal of Structural Chemistry, 2010. **51**(6): p. 1126-1131.
12. Yang, J., H. Sun, and C. Chen, *Is Osmium Diboride An Ultra-Hard Material?* Journal of the American Chemical Society, 2008. **130**(23): p. 7200-7201.
13. STUBICAR, M., A. TONEJC, and N. STUBICAR, *X–RAY DIFFRACTION STUDY OF W–B ELEMENTAL POWDER MIXTURES AFTER HIGH–ENERGY BALL–MILLING1.* Fizika A, 1995. **4**(1): p. 65-72.
14. Khor, K.A., L.G. Yu, and G. Sundararajan, *Formation of hard tungsten boride layer by spark plasma sintering boriding.* Thin Solid Films, 2005. **478**(1): p. 232-237.
15. Kawanowa, H., et al., *Structure analysis of the WB2(0001) surface.* Surface Science, 1999. **433-435**: p. 661-665.
16. Usta, M., et al., *The characterization of borided pure tungsten.* Surface and Coatings Technology, 2005. **194**(2): p. 330-334.
17. Cai, K.-f. and C.-W. Nan, *The influence of W2B5 addition on microstructure and thermoelectric properties of B4C ceramic.* Ceramics International, 2000. **26**(5): p. 523-527.
18. Stadler, S., et al., *Electronic structures of the tungsten borides WB, W2B and W2B5.* Journal of Electron Spectroscopy and Related Phenomena, 2000. **110-111**: p. 75-86.
19. Humphry-Baker, S.A. and G.D.W. Smith, *Shielding materials in the compact spherical tokamak.* 2019. **377**(2141): p. 20170443.
20. Windsor, C.G., et al., *Design of cemented tungsten carbide and boride-containing shields for a fusion power plant.* Nuclear Fusion, 2018. **58**(7): p. 076014.
21. Sykes, A., et al., *Compact fusion energy based on the spherical tokamak.* Nuclear Fusion, 2017. **58**(1): p. 016039.
22. Windsor, C.G., et al., *Tungsten boride shields in a spherical tokamak.* Nuclear Fusion, 2021. **61**: p. 086018.
23. Kieffer, R. and F. Benesovsky, *In Hartstoffe.* Vienna: Springer-Verlag, 1963.

24. Kiessling, R., *The Crystal Structures of Molybdenum and Tungsten Borides.* Acta Chem. Scand., 1947. **1**.
25. Itoh, H., et al., *Formation process of tungsten borides by solid state reaction between tungsten and amorphous boron.* Journal of Materials Science, 1987. **22**(8): p. 2811-2815.
26. Okada, S., K. Kudou, and T. Lundström, *Preparations and Some Properties of W2B, δ -WB and WB2 Crystals from High-Temperature Metal Solutions.* Japanese Journal of Applied Physics, 1995. **34**(Part 1, No. 1): p. 226-231.
27. Woods, H.P., J. F. E. Wagner, and B. G. Fox, *Tungsten diboride, preparation and structure.* Science, 1966. **151**.
28. Kayhan, M., et al., *Neutron diffraction and observation of superconductivity for tungsten borides, WB and W2B4.* Solid State Sciences, 2012. **14**(11): p. 1656-1659.
29. Mohammadi, R., et al., *Tungsten tetraboride, an inexpensive superhard material.* 2011. **108**(27): p. 10958-10962.
30. Li, Q., et al., *Global Structural Optimization of Tungsten Borides.* Physical Review Letters, 2013. **110**(13): p. 136403.
31. Lundstrom, T., *The structure of Ru2B3 and WB2. 0 as determined by single-crystal diffractometry, and some notes on the WB system.* Ark. Kemi,, 1969. **30**: p. 115–127.
32. Romans, P.A. and M.P. Krug, *Composition and crystallographic data for the highest boride of tungsten.* Acta Cryst, 1966. **20**: p. 313-315.
33. Kayhan, M., *Transition metal borides Synthesis, characterization and superconducting properties*. 2013.
34. Kresse, G. and J. Hafner, *Ab initio molecular dynamics for liquid metals.* Physical Review B, 1993. **47**(1): p. 558-561.
35. Kresse, G. and J. Hafner, *Ab initio molecular-dynamics simulation of the liquid-metal--amorphous-semiconductor transition in germanium.* Physical Review B, 1994. **49**(20): p. 14251-14269.
36. Kresse, G. and J. Furthmüller, *Efficiency of ab-initio total energy calculations for metals and semiconductors using a plane-wave basis set.* Computational Materials Science, 1996. **6**(1): p. 15-50.
37. Perdew, J.P. and A. Zunger, *Self-interaction correction to density-functional approximations for many-electron systems.* Physical Review B, 1981. **23**(10): p. 5048-5079.
38. Perdew, J.P., K. Burke, and M. Ernzerhof, *Generalized Gradient Approximation Made Simple.* Physical Review Letters, 1996. **77**(18): p. 3865-3868.
39. Blöchl, P.E., *Projector augmented-wave method.* Physical Review B, 1994. **50**(24): p. 17953-17979.
40. Kresse, G. and D. Joubert, *From ultrasoft pseudopotentials to the projector augmented-wave method.* Physical Review B, 1999. **59**(3): p. 1758-1775.
41. Monkhorst, H.J. and J.D. Pack, *Special points for Brillouin-zone integrations.* Physical Review B, 1976. **13**(12): p. 5188-5192.
42. Methfessel, M. and A.T. Paxton, *High-precision sampling for Brillouin-zone integration in metals.* Physical Review B, 1989. **40**(6): p. 3616-3621.
43. Fultz, B., *Vibrational thermodynamics of materials.* Progress in Materials Science, 2010. **55**(4): p. 247-352.
44. Giannozzi, P., et al., *Ab initio calculation of phonon dispersions in semiconductors.* Physical Review B, 1991. **43**(9): p. 7231-7242.
45. Togo, A. and I. Tanaka, *First principles phonon calculations in materials science.* Scripta Materialia, 2015. **108**: p. 1-5.

46. Hill, R., *The Elastic Behaviour of a Crystalline Aggregate.* Proceedings of the Physical Society. Section A, 1952. **65**(5): p. 349-354.
47. Voigt, W., *Lehrbuch der Kristallphysik.* Teubner Verlag, Leipzig., 1928.
48. Reuss, A., *Berechnung der Fließgrenze von Mischkristallen auf Grund der Plastizitätsbedingung für Einkristalle.* 1929. **9**(1): p. 49-58.
49. Toby, B.H. and R.B. Von Dreele, *GSAS-II: the genesis of a modern open-source all purpose crystallography software package.* Journal of Applied Crystallography, 2013. **2**(46): p. 544-549.
50. Ghosh, G., A. van de Walle, and M. Asta, *First-principles calculations of the structural and thermodynamic properties of bcc, fcc and hcp solid solutions in the Al–TM (TM=Ti, Zr and Hf) systems: A comparison of cluster expansion and supercell methods.* Acta Materialia, 2008. **56**(13): p. 3202-3221.
51. Zhang, X., G. Trimarchi, and A. Zunger, *Possible pitfalls in theoretical determination of ground-state crystal structures: The case of platinum nitride.* Physical Review B, 2009. **79**(9): p. 092102.
52. Zhao, C., et al., *Unexpected stable phases of tungsten borides.* Physical Chemistry Chemical Physics, 2018. **20**(38): p. 24665-24670.
53. Setayandeh, S.S., et al., *Effect of pseudopotential choice on the calculated electron and phonon band structures of palladium hydride and its vacancy defect phases.* International Journal of Hydrogen Energy, 2021. **46**(1): p. 943-954.
54. Alers, G.A. and J.R. Neighbours, *Crystal Stability and Elastic Constants.* 1957. **28**(12): p. 1514-1514.
55. Mouhat, F. and F.-X. Coudert, *Necessary and sufficient elastic stability conditions in various crystal systems.* Physical Review B, 2014. **90**(22): p. 224104.
56. Born, M. and K. Huang, *In Dynamical Theory of Crystal Lattices*. 1954: Oxford: Clarendon Press.
57. Liu, Q.-J., et al., *First-principles calculations of structural, elastic, and electronic properties of trigonal ZnSnO3 under pressure.* Materials Chemistry and Physics, 2016. **180**: p. 75-81.
58. McSkimin, H.J. and P. Andreatch, *Elastic Moduli of Diamond as a Function of Pressure and Temperature.* Journal of Applied Physics, 1972. **43**(7): p. 2944-2948.
59. Cheng, X.Y., et al., *Computational materials discovery: the case of the W-B system.* Acta Crystallogr C Struct Chem, 2014. **70**(Pt 2): p. 85-103.
60. Li, P., et al., *Elastic anisotropies and thermal conductivities of WB2 diborides in different crystal structures: A first-principles calculation.* Journal of Alloys and Compounds, 2018. **747**: p. 905-915.
61. Nye, J.F., *In Physical Properties of Crystals*. 1979: Oxford University Press.
62. Pugh, S.F., *XCII. Relations between the elastic moduli and the plastic properties of polycrystalline pure metals.* The London, Edinburgh, and Dublin Philosophical Magazine and Journal of Science, 1954. **45**(367): p. 823-843.
63. Pettifor, D.G., *Theoretical predictions of structure and related properties of intermetallics.* Materials Science and Technology, 1992. **8**(4): p. 345-349.
64. Huang, B., et al., *Electronic structures, mechanical and thermodynamic properties of cubic alkaline-earth hexaborides from first principles calculations.* Journal of Alloys and Compounds, 2015. **635**: p. 213-224.
65. Meschel, S.V. and O.J. Kleppa, *Standard Enthalpies of Formation of NbB2, MoB, and ReB2 by High-Temperature Direct Synthesis Calorimetry.* Metall. Mater. Trans. A, 1993. **24**: p. 947.
66. Burr, P.A. and S.X. Oliver, *Formation and migration of point defects in tungsten carbide: Unveiling the sluggish bulk self-diffusivity of WC.* Journal of the European Ceramic Society, 2019. **39**(2): p. 165-172.
67. Iwasawa, M., et al., *First-Principles Calculation of Point Defects in Uranium Dioxide.* Materials Transactions - MATER TRANS, 2006. **47**: p. 2651-2657.